Electronic Supplementary Material (ESI) for Nanoscale.

Supplementary information

Near-Infrared Two-Photon Excited Photoluminescence from Yb^{3+}-Doped $CsPbCl_xBr_{3-x}$ Perovskite Nanocrystals Embedded into Amphiphilic Silica Microspheres

Danila A. Tatarinov,[a] Ivan D. Skurlov,[a] Anastasiia V. Sokolova,[b] Alexander A. Shimko,[c] Denis V. Danilov,[c] Yuliya A. Timkina,[a] Maxim A. Rider,[a] Viktor V. Zakharov,[a] Sergey A. Cherevkov,[a] Natalya K. Kuzmenko,[d] Aleksandra V. Koroleva,[c] Evgeniy V. Zhizhin,[c] Nadezhda A. Maslova,[c] Ekaterina Yu. Stovpiaga,[a] Dmitry A. Kurdyukov,[a] Valery G. Golubev,[a] Xiaoyu Zhang,[e] Weitao Zheng,[e] Anton N. Tcypkin,[f] Aleksandr P. Litvin,* [a,e,f] and Andrey L. Rogach.[b]

[a] PhysNano Department, ITMO University, St. Petersburg, 197101 Russia.

[b] Department of Materials Science and Engineering, and Center for Functional Photonics, City University of Hong Kong, Hong Kong SAR, 999077 China

[c] Research Park, Saint Petersburg State University, St. Petersburg, 199034 Russia

[d] Research Center for Optical Materials Science, ITMO University, Saint Petersburg, 197101 Russia.

[e] Key Laboratory of Automobile Materials MOE, School of Materials Science & Engineering, and Jilin Provincial International Cooperation Key Laboratory of High-Efficiency Clean Energy Materials, Jilin University, Changchun 130012, China

[f] Laboratory of Quantum Processes and Measurements, ITMO University, Saint Petersburg, 197101 Russia

* litvin@jlu.edu.cn

Supplement Figures

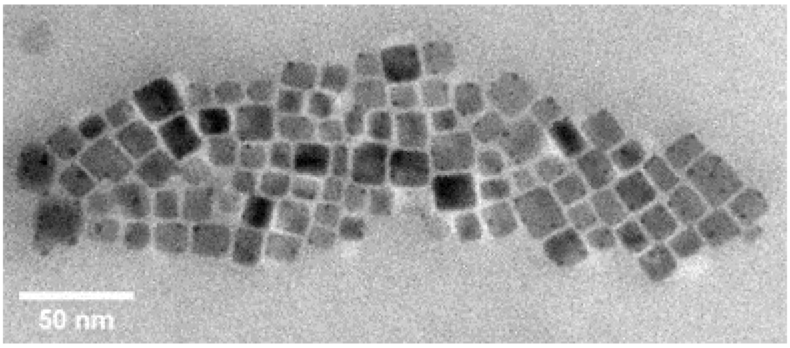

Fig. S1. TEM image of Yb^{3+}:$CsPbCl_3$ NCs.

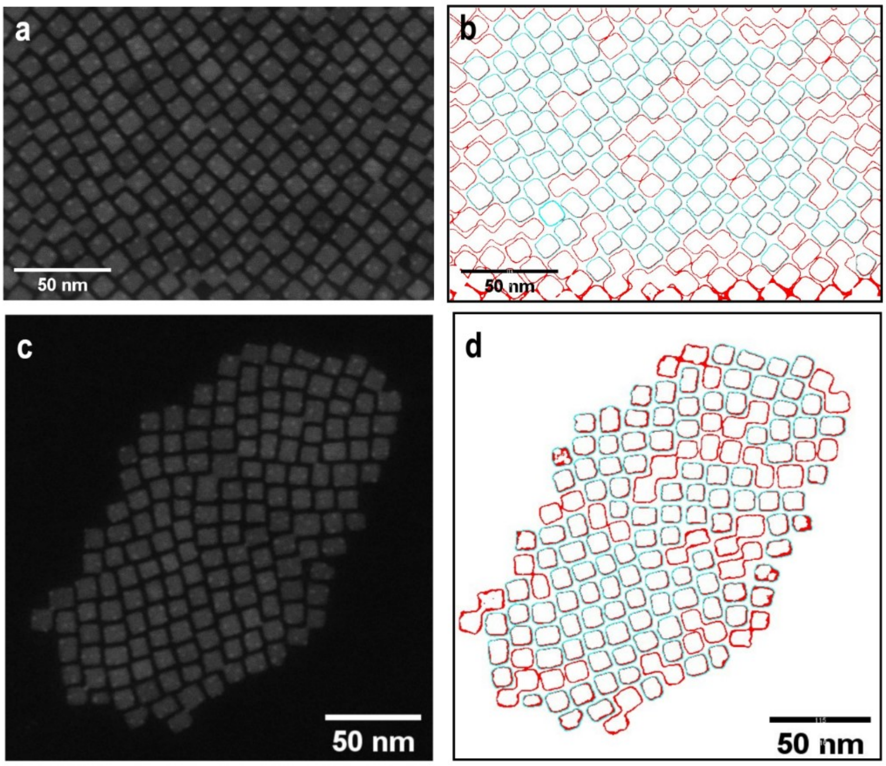

Fig. S2. HAADF-STEM images (a, c) of Yb^{3+}:$CsPbCl_3$ NCs and (b, d) estimation of their area using ImageJ software. The blue counter indicates counted NCs, while the red counter indicates non-counted (merged or border-sharing) NCs. An average edge length was calculated as a root square of the average counted area.

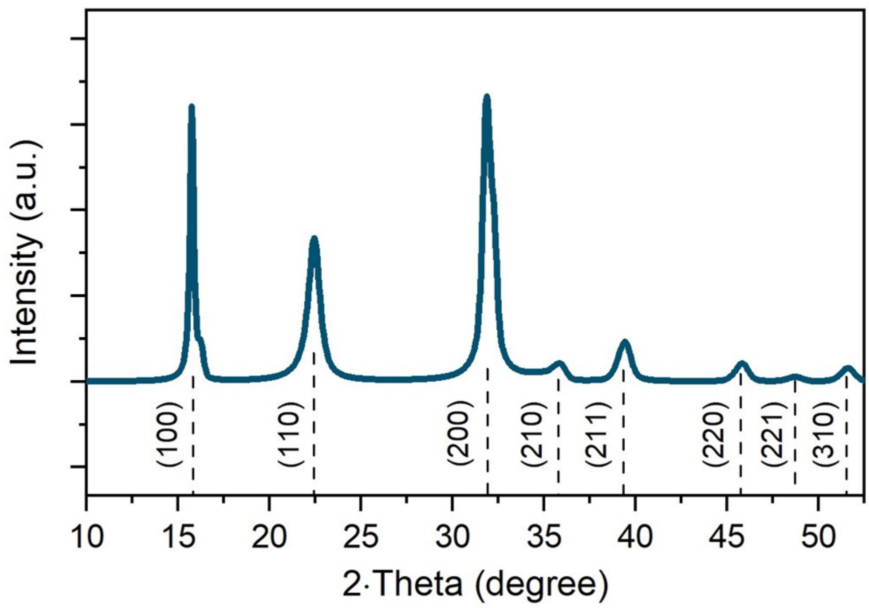

Fig. S3. XRD pattern of the synthesized Yb^{3+}:$CsPbCl_3$ NCs compared to the reference (vertical dashed lines) $CsPbCl_3$ cubic perovskite phase (PDF Card No. 01-075-0411).

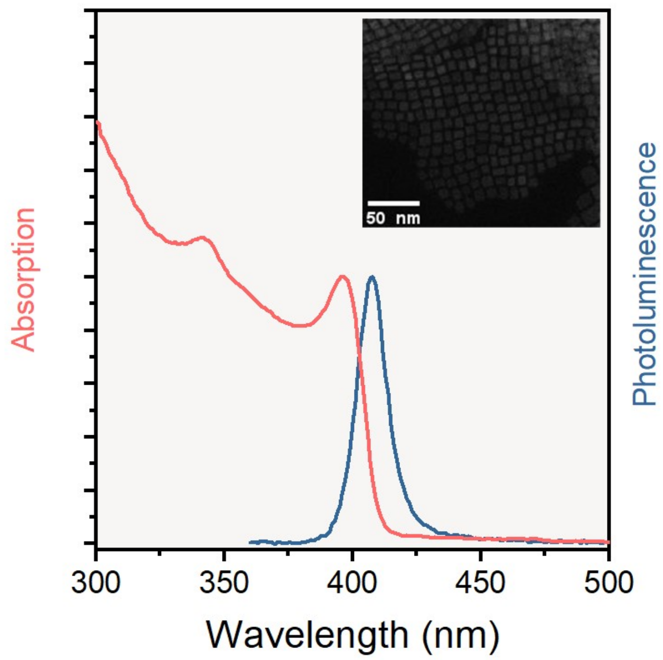

Fig. S4. Absorption and PL spectra of the undoped $CsPbCl_3$ NCs. The inset shows their HAADF-STEM image.

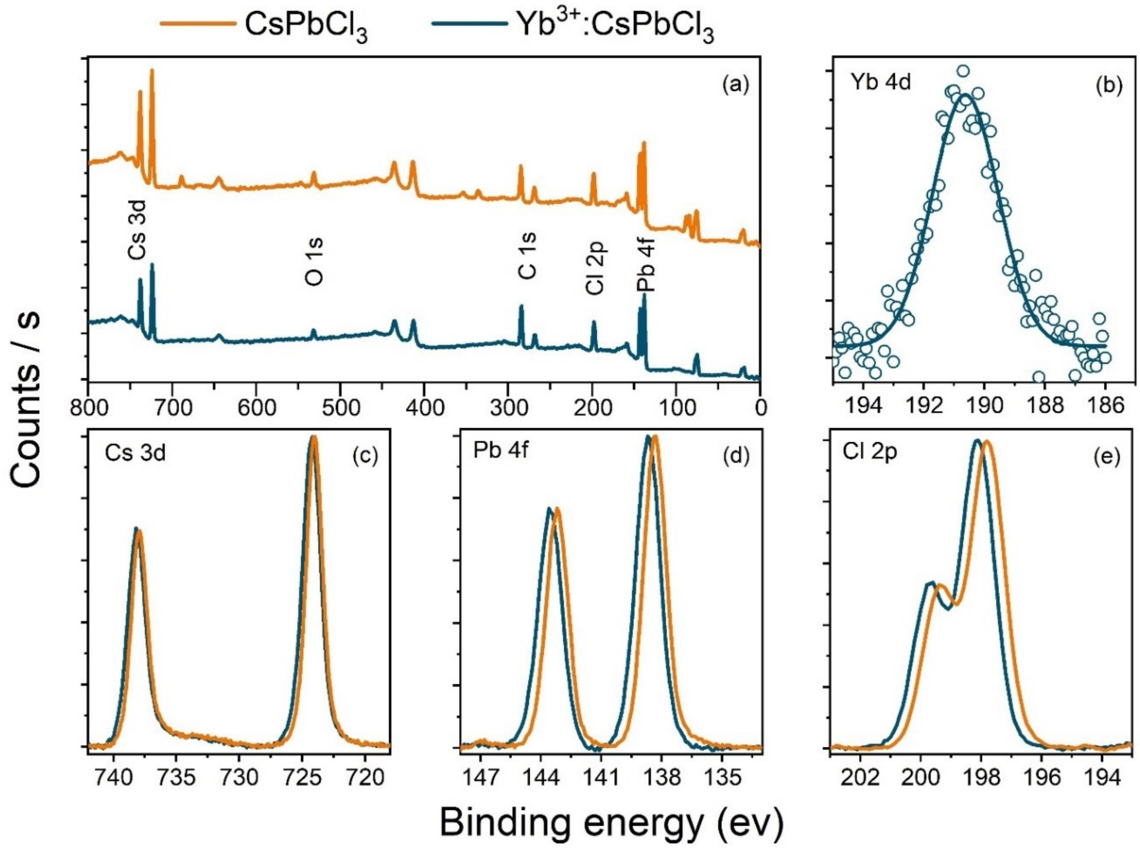

Fig. S5. (a) Survey XPS spectra for the undoped $CsPbCl_3$ (orange line) and doped $Yb^{3+}:CsPbCl_3$ (blue line) NCs. (b) High-resolution XPS spectra of the Yb 4d peak for the doped $Yb^{3+}:CsPbCl_3$ NCs. High-resolution XPS spectra for Cs 3d (c), Pb 4f (d), and Cl 2p (e) peaks for the undoped $CsPbCl_3$ (orange lines) and doped $Yb^{3+}:CsPbCl_3$ (blue lines) NCs.

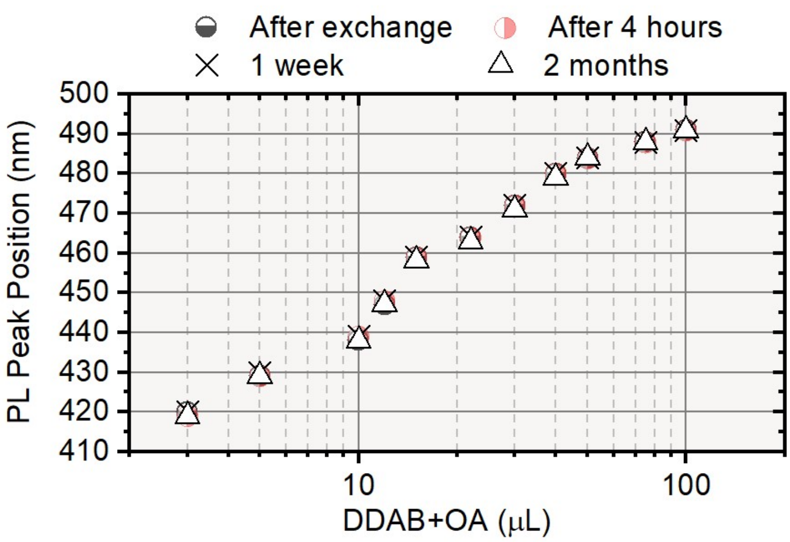

Fig. S6. Stability of the band-edge PL peak positions for the $Yb^{3+}:CsPbCl_xBr_{3-x}$ NCs after an anion exchange.

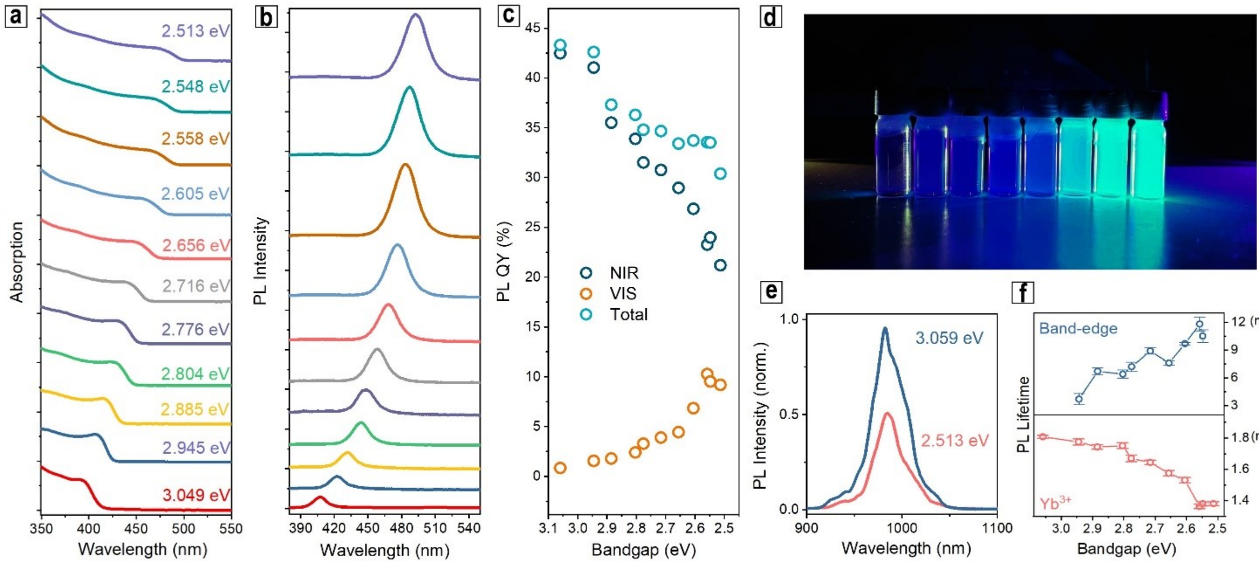

Fig. S7. (a) Absorption and (b) PL spectra of Yb^{3+}:$CsPbCl_xBr_{3-x}$ NCs in the visible spectral range upon anion exchange. The numbers on (a) provide their bandgaps (in eV) estimated from the Tauc plots; the color coding for the spectra in (a) and (b) is the same. (c) Dependencies of visible, NIR, and total PL QY on the bandgap of the Yb^{3+}:$CsPbCl_xBr_{3-x}$ NCs. (d) Photograph of Yb^{3+}:$CsPbCl_xBr_{3-x}$ NC solutions with varying bandgaps, taken under UV illumination. (e) NIR spectra of NCs with bandgaps of 3.059 eV (Yb^{3+}:$CsPbCl_3$) and 2.513 eV (Yb^{3+}:$CsPbCl_xBr_{3-x}$). (f) Dependencies of the BE and Yb^{3+}-related PL lifetimes on the NC bandgap.

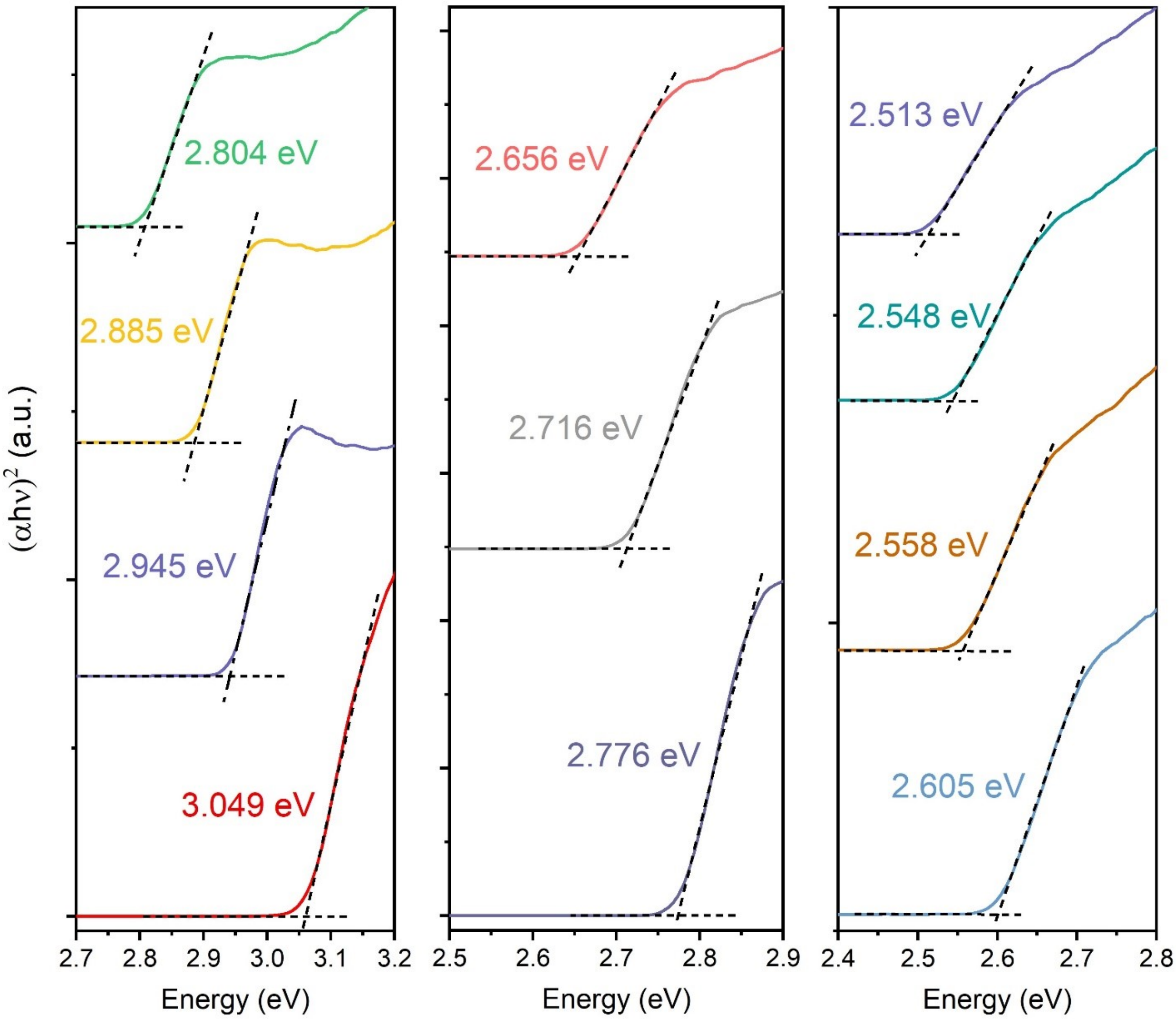

Fig. S8. Tauc plots for the Yb^{3+}:$CsPbCl_xBr_{3-x}$ NCs shown in Fig. S6. The bandgaps were calculated as an intercept of the slope's linear fit with a zero line.

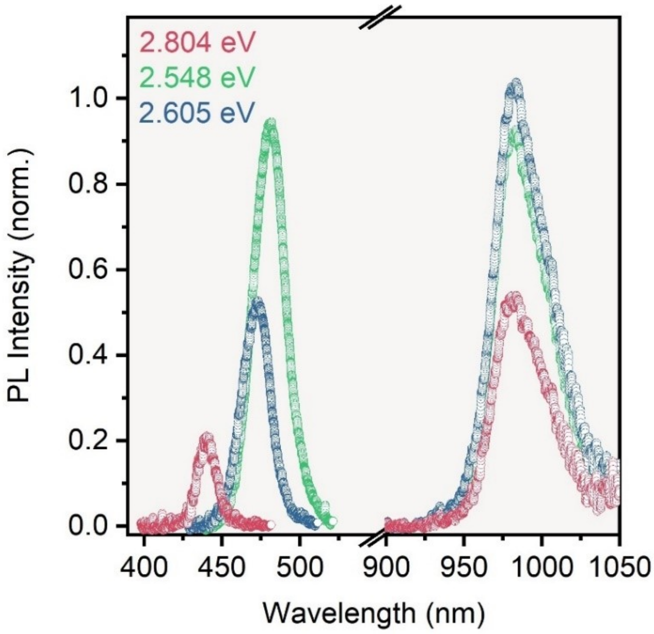

Fig. S9. PL spectra of the Yb^{3+}:$CsPbCl_xBr_{3-x}$ NCs with different bandgaps (marked with numbers on the frame) taken under two-photon (800 nm) excitation and corrected to the spectral sensitivity of the detection system.

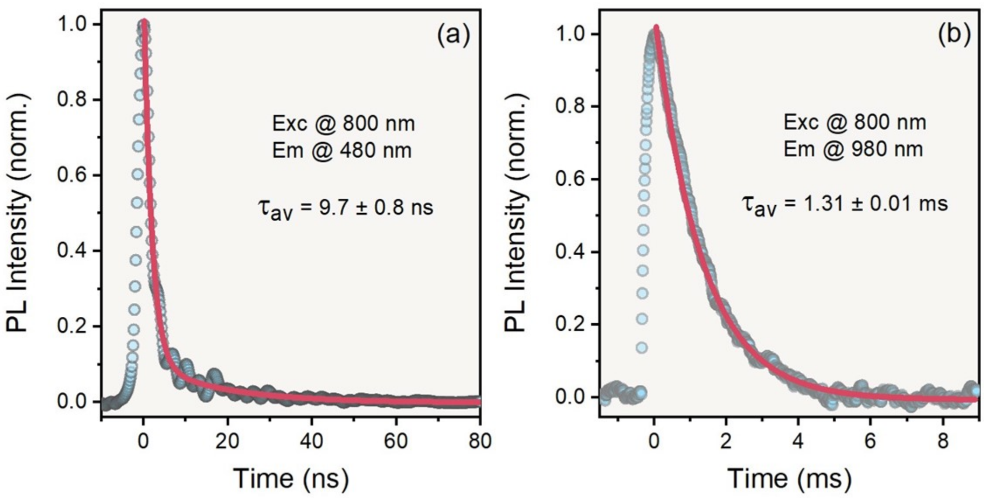

Fig. S10. PL decay kinetics recorded under 800 nm excitation for the band-edge related (a) and Yb^{3+}-related (b) emissions for Yb^{3+}:$CsPbCl_3$ NCs. Solid lines are two- (a) and one-exponential (b) fits, respectively.

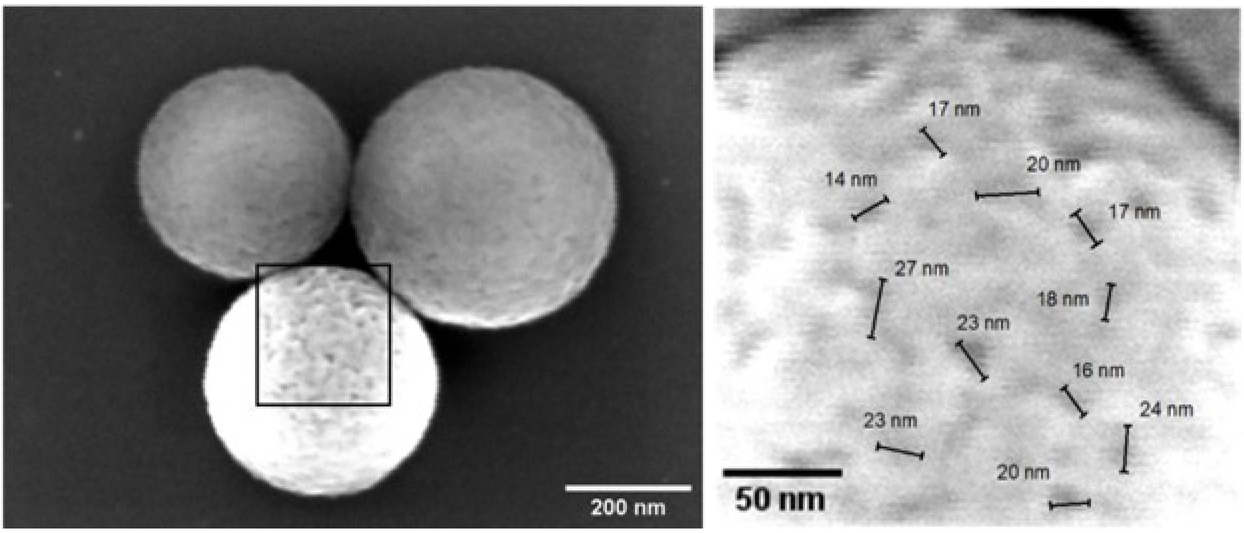

Fig. S11. Estimation of MS pores size from their SEM images.

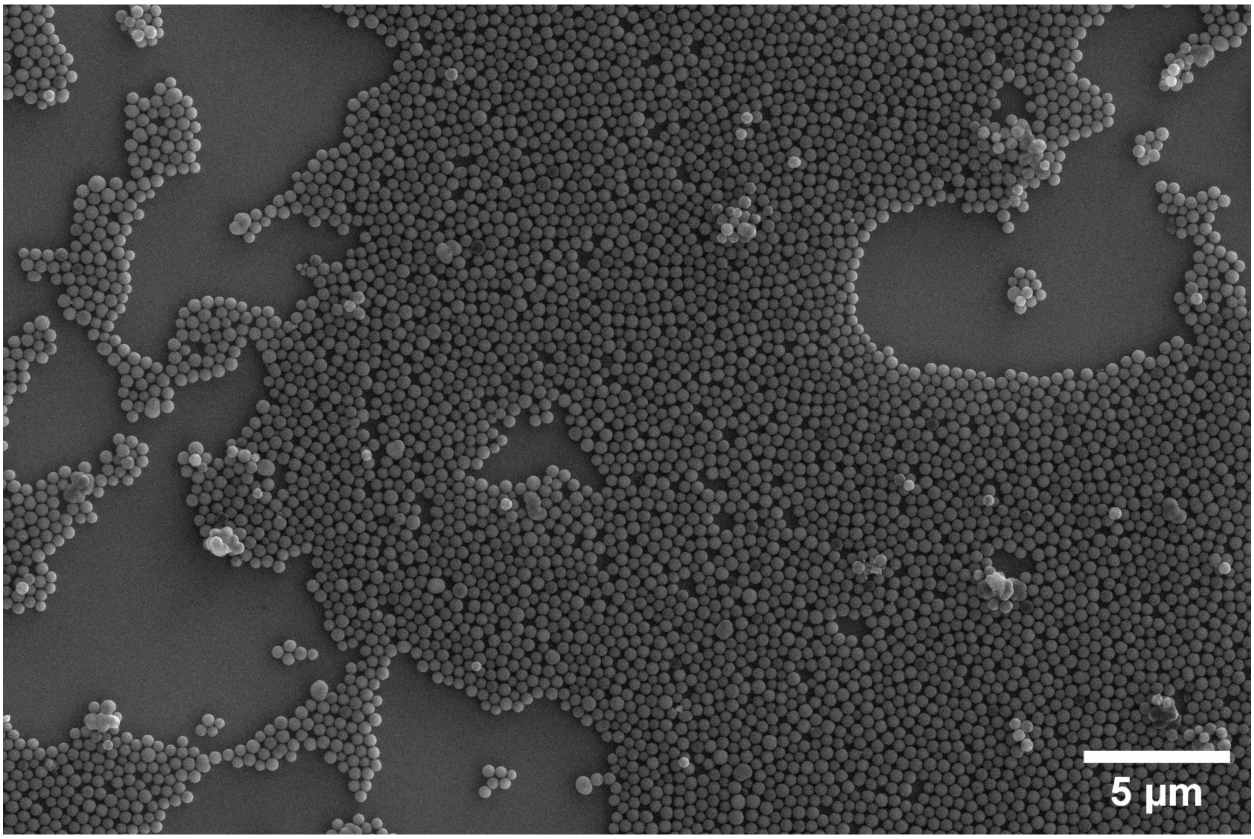

Fig. S12. Large-area SEM image of MS with embedded Yb^{3+}:$CsPbCl_3$ NCs, spread over Si substrate.

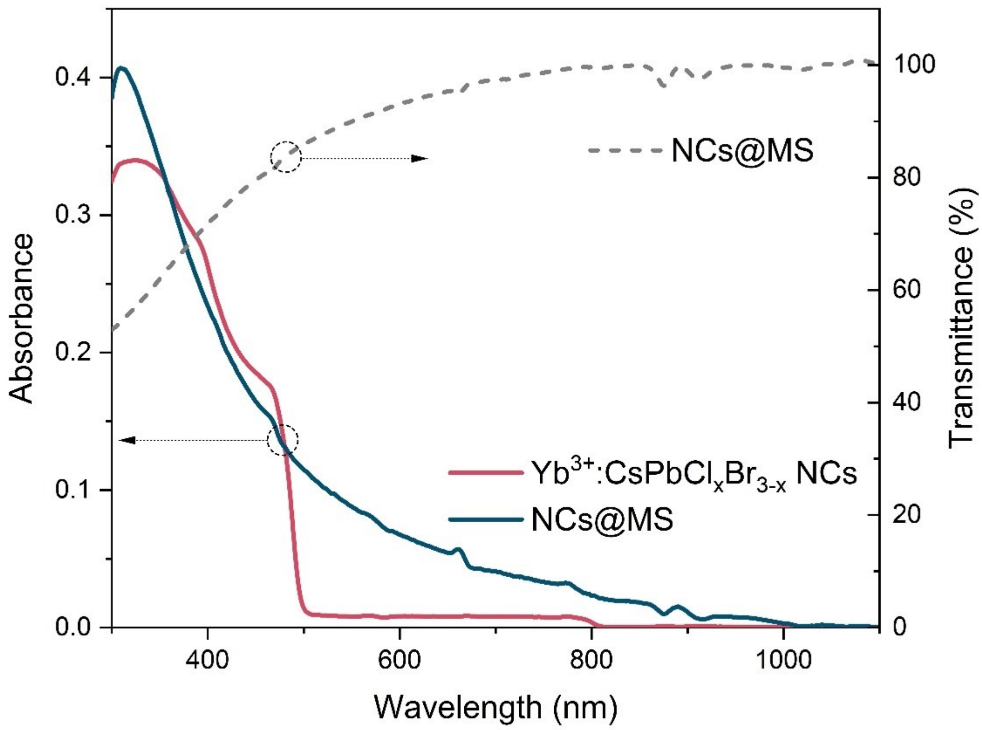

Fig. S13. Absorption spectra (solid lines) of Yb^{3+}:$CsPbCl_3$ NCs and those NCs embedded into MS (NCs@MS), and transmittance spectrum (dashed line) of the latter.

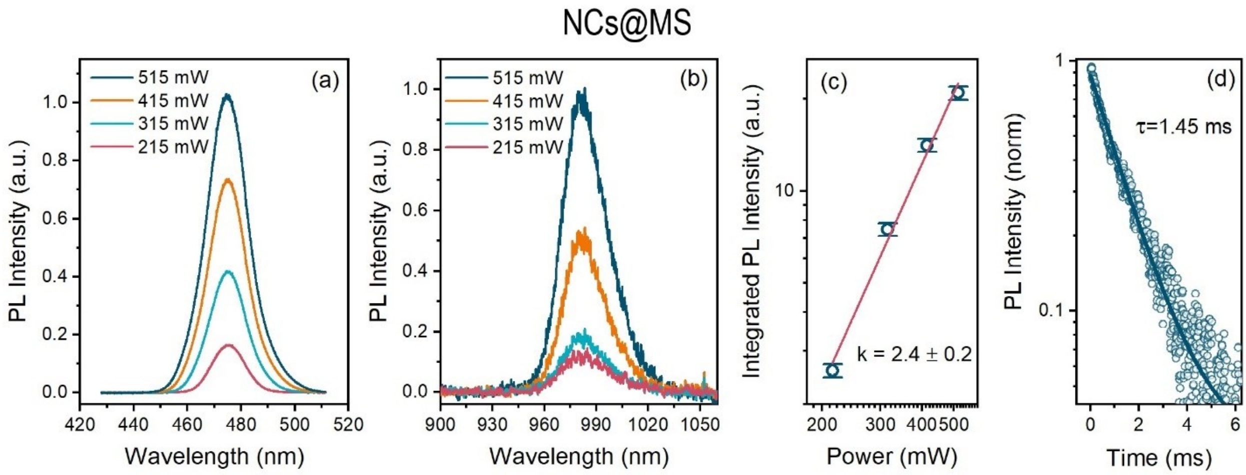

Fig. S14. PL spectra of the Yb^{3+}: $CsPbCl_xBr_{3-x}$ NCs embedded in MS (NCs@MS), measured under two-photon excitation (800 nm) in the visible (a) and NIR (b) spectral ranges. (c) Dependence of the integrated PL intensity of the NCs@MS on the excitation power. The slope of 2.4±0.2 is close to that expected for the TPA excitation process. (d) PL decay curve recorded for the Yb^{3+}-related emission of the NCs@MS in the NIR spectral range. The average PL lifetime of 1.45 ms corresponds to that obtained for the Yb^{3+}: $CsPbCl_xBr_{3-x}$ NCs in colloidal solution (Fig. S7f).

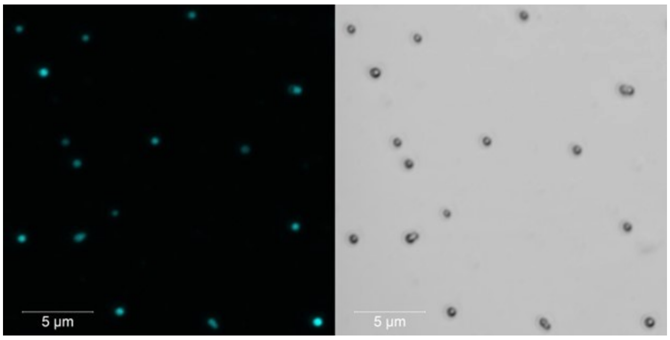

Fig. S15. Large-area luminescence (left) and transmitted light (right) images of NCs@MS obtained by CLSM.

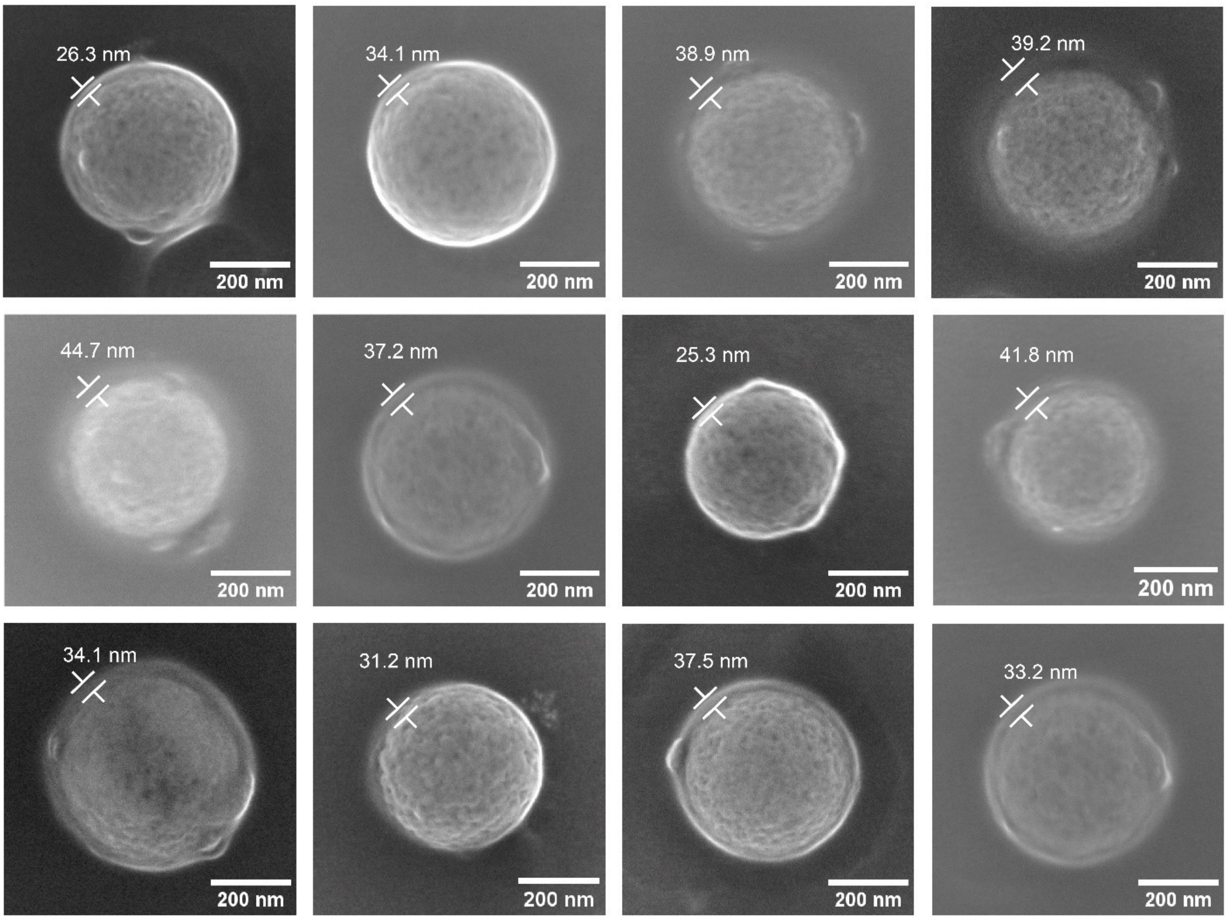

Fig. S16. SEM images of NCs@MS covered with PEG.

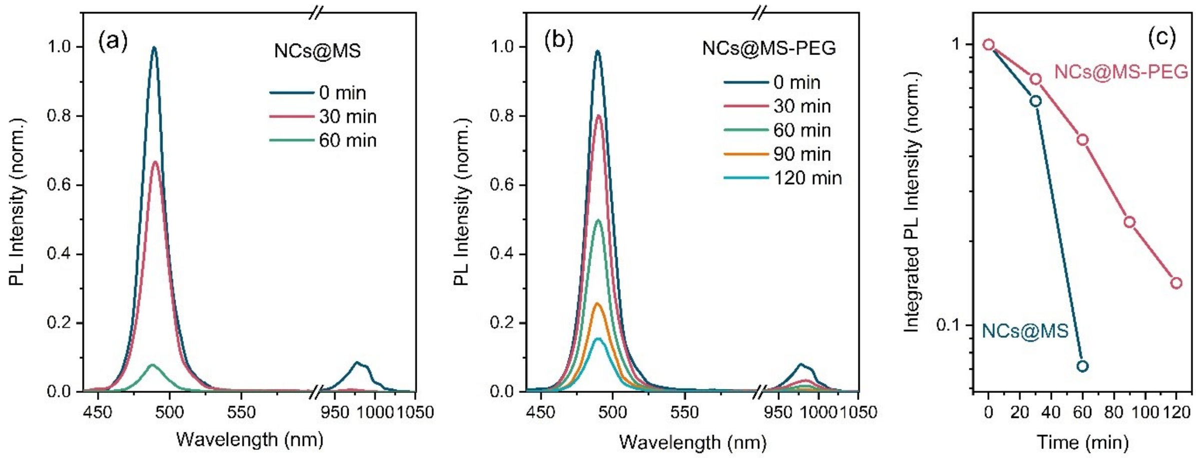

Fig. S17. Stability of PL response in water for NCs@MS without and with PEG functionalization. PL spectra taken for NCs@ MS without (a) and with (b) PEG functionalization after the specified periods of time. (c) The dependencies of integrated PL intensities over time in water for NCs@MS without (blue) and with (red) PEG functionalization.

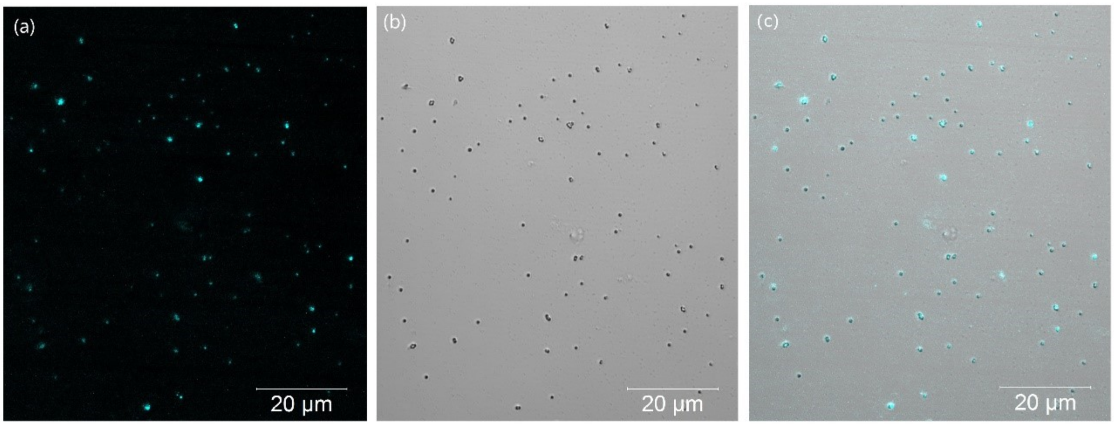

Fig. S18. Large-area luminescence (a), transmitted light (b), and superimposed (c) images of the NCs@MS covered with PEG obtained by CLSM.

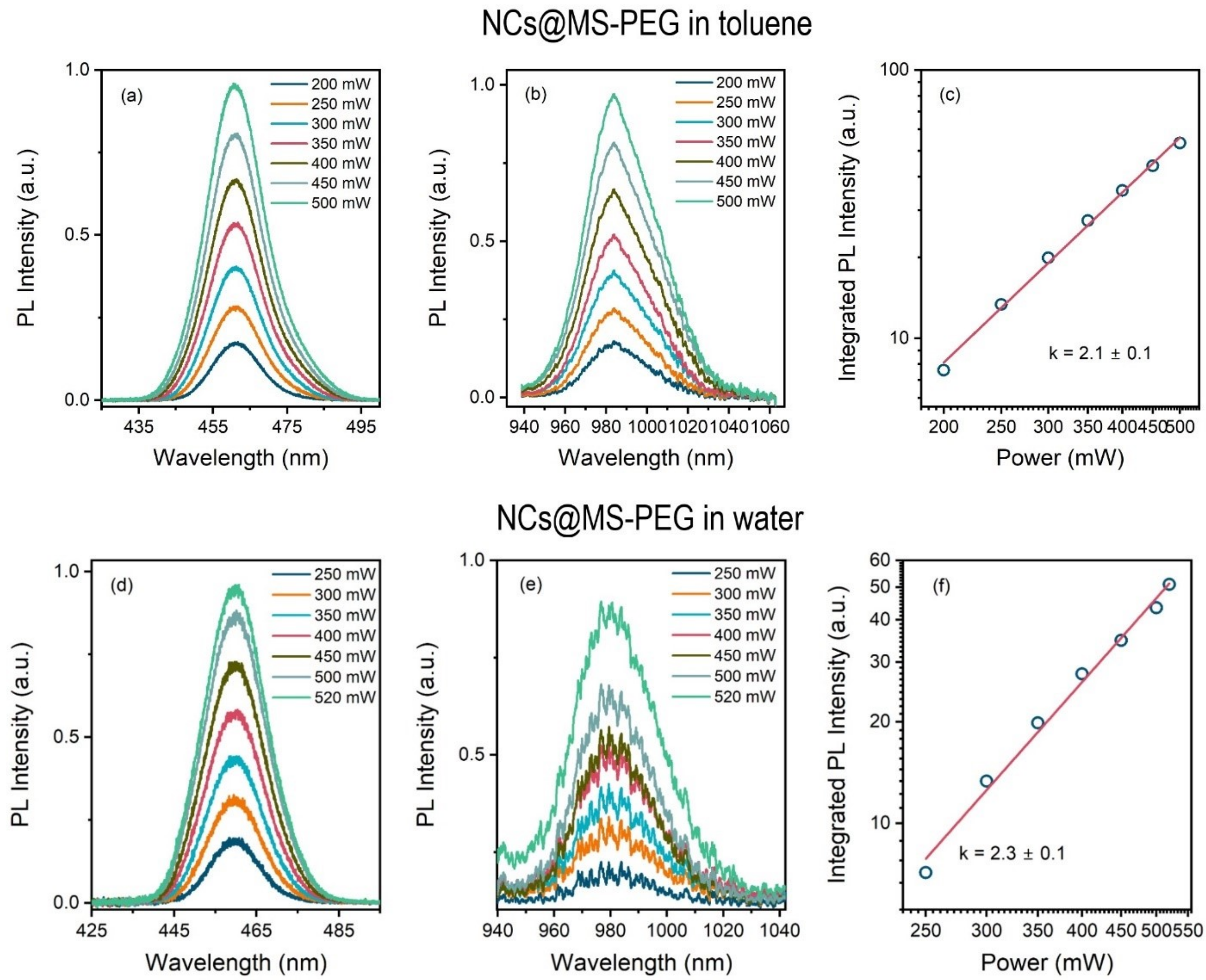

Fig. S19. PL spectra in the visible (a, d) and NIR (b, e) spectral regions taken from NCs@MS covered with PEG and dispersed in toluene (upper panel) and water (bottom panel) under TPA-excitation. (c, f) Corresponding dependencies of the integrated PL intensity upon the excitation power; the slopes confirm occurrence of the TPA excitation.

Supplement Tables

Table S1. Key optical properties of the Yb^{3+}:$CsPbCl_xBr_{3-x}$ NCs obtained by anion-exchange.

DDAB amount, µL	Bandgap, eV	BE-PL peak position, nm	Visible PL QY, %	NIR PL QY, %	Total PL QY, %	TPA slope	σ, $\times 10^5$ GM
0	3.049	407	0.8	42.5	43.3	–	0.10
2	2.945	422	1.6	41.1	42.7	1.9	0.15
4	2.885	431	1.8	35.5	37.3	2.0	0.31
8	2.804	444	2.4	33.9	36.3	2.3	0.98
12	2.776	448	3.3	31.5	34.8	2.1	1.01
16	2.716	459	3.9	30.8	34.7	2.3	1.41
24	2.656	468	4.5	28.9	33.4	2.2	1.70
32	2.605	476	6.8	26.9	33.7	2.2	1.84
40	2.558	483	10.3	23.3	33.6	2.3	2.06
48	2.548	487	9.5	24.0	33.5	2.3	2.34
64	2.513	493	9.2	21.2	30.4	2.2	2.21

Table S2. Examples of previously reported values of TPA cross-sections for $CsPbCl_xBr_{3-x}$ perovskite nanostructures of different compositions and shapes, measured under 800 nm excitation. Mixed-halide structures are marked in bold.

Composition	Shape	σ, GM	Method	Emission peak, nm	Year	Ref.
$CsPbClBr_2$	NCs	**1.6×10^5**	Z-scan	471	2018	1
$CsPbCl_2Br$	NCs	**1.1×10^5**		451		
$CsPbBr_3$	NCs	2.2×10^5		527		
$CsPbCl_{0.6}Br_{2.4}$	Nanorods	**1.2×10^6**	Z-scan	502	2020	2
$CsPbBr_3$	Nanorods	1.5×10^6		520		
CsPbCl	NCs	3.8×10^4	TPA-PL	410	2019	3
$CsPbBr_{1.5}Cl_{1.5}$	NCs	**8.8×10^4**		475		
$CsPbBr_3$	NCs	1.8×10^5		535		
$CsPbBr_3$	NCs	2.7×10^6	Z-scan	520	2016	4
$CsPbBr_3$	NCs	1.2×10^5	Z-scan	515	2016	5
$CsPbBr_3$	NCs	2.0×10^6	Z-scan	520	2017	6
$CsPbBr_3$	NCs	3.2×10^5	TPA-PL	515	2021	7
$CsPb_{0.78}Cd_{0.22}Br_3$	NCs	2.6×10^6	TPA-PL	510		
$CsPbBr_3$	NCs	4×10^5	TPA-PL	525	2022	8
$CsPb_{0.93}Cd_{0.07}Br_3$	NCs	4.5×10^5		523		
$CsPb_{0.88}Cd_{0.12}Br_3$	NCs	$5÷6 \times 10^5$		521		
$CsPbBr_3$	Nanoplates	4.8×10^5	TPA-PL	484	2020	9
$CsPbBr_3$	NCs	8.1×10^4		528		
$CsPbBr_3$	Nanowires	2.3×10^5		534		
Yb^{3+}: **$CsPbCl_xBr_{3-x}$**	NCs	**$0.1–2.3 \times 10^5$**	TPA-PL	407-490 nm + 985 nm	2024	**This work**

Table S3. Comparison of stability in water for perovskite-based composite materials, according to literature data.

Materials	Method of synthesis	PL peak position	PL QY (non-polar solvent)	Size	PL stability	Application	Year	Ref.
$CsPbBr_3/mSiO_2$ composites	LARP	510 nm	90%	10 nm	50% after 35 days (H_2O)	LEDs	2020	[10]
$CsPbBr_3/mSiO_2$ nanocomposites	*in situ* template-assisted synthesis	514 nm	63%	150 nm	100% after 50 days (H_2O)	Biosensing	2024	[11]
$CsPbBr_3$-SiO_2 composites	One-step *in-situ* synthesis and encapsulation method	520 nm	84.7%	Thin films with 34.7 nm crystals	＞60% for 1100 h (H_2O)	N/A	2023	[12]
$CsPbBr_3$/ SiO_2 nanocrystals	RT synthesis and SiO_2 encapsulation	520 nm	N/A	140 nm	98.3% after 168 h (H_2O)	PL sensing	2022	[13]
$CsPbBr_3$ QDs/MSs	High temperature solid phase melting method	520 nm	N/A	500 nm	80% for 2 weeks (H_2O)	WLEDs	2022	[14]
$CsPbBr_3$/ SiO_2 composites	Molten salts synthesis approach	520 nm	89 ± 10%	0.6 μm	95% after 30 days (H_2O)	WLEDs	2021	[15]
DDAB-$CsPbBr_3$/ SiO_2 QDs composites	Silica-coating at room temperature	520 nm	80%	N/A	50% after 210 min (H_2O)	WLEDs	2021	[16]
$CsPbBr_3$/ polymer microspheres	Encapsulation in microspheres	520 nm	N/A	285 nm	100% after 28 days (H_2O)	Detectors	2021	[17]

$CsPbBr_3$-SiO_2 powders	Encapsulating derived from molecular sieve templates at high temperature	520 nm	63%	Pore size 3.6 nm length N/A	100% after 50 days (H_2O)	LEDs	2020	[18]
$CsPbBr_3$/mSiO_2 composites	Hot injection *in situ* growth in m-SiO2 matrix	520 nm	68%	400 nm	80% after 120 h (H_2O)	Flexible LEDs	2019	[19]
$CsPbBr_3$/mSiO_2 composites	HI+ SiO_2 coating with MPTMS	525 nm	80%	150 nm	80% after 13 h (H_2O)	TPA-excited PL	2020	[20]
$CsPbX_3$@SiO_2 nanocomposites	HI+ SiO_2 coating with TEOS	410-680 nm	9%-84%	100 nm	60%-95% after 30 days (H_2O)	LEDs and cell imaging	2018	[21]
$APbX_3$/meso-SiO_2	*in situ* template-assisted synthesis	480-620 nm	48%-90%	Pore size 2.5-7 nm, length N/A	N/A	N/A	2016	[22]
$CsPbX_3$/meso-SiO_2 spheres	NCs encapsulation	450-640 nm	≤55%	N/A	N/A	WLEDs	2016	[23]
$FAPbI_3$@ SiO_2 composites	LARP+ TOPO	770 nm	72%	15 nm	80% after 28 days (atmosphere)	LEDs	2023	[24]
$CsPbI_3$@SiO_2 composites	HI+ SiO_2 coating	660 - 680nm	97.5%	10.07± 0.93 nm	79% PL retention after 40 min (ethanol)	NIR LEDs	2023	[25]

$CsPbI_3@SiO_2$ nanocomposites	HI+ SiO_2 coating with APTES	697 nm	N/A	13 nm	95% after 48 h (H_2O)	LEDs	2019	[26]
$FAPbI_3@$ TEOS	LARP+ TEOS	770 nm	57.2%	15.17 nm	80% PL retention after 7 days (Toluene/DI H_2O)	NIR LEDs	2023	[27]
$MAPbBr_xI_{x-3}$/ meso-SiO_2	*in situ* template-assisted synthesis	500-800 nm	≤5.5%	Pore size 3.3-7.1 nm, length N/A	N/A	Solid-state LEDs	2016	[28]
$FAPbI_3@$ APTES	LARP+ APTES	770 - 810nm	58 %	16.8 nm	30% PL retention after 380 min (Toluene/DI H_2O)	NIR LEDs	2021	[29]
Yb^{3+}: $CsPbCl_xBr_{3-x}$ @MSs@PEG	Encapsulation in MSs+PEG	407-490 + 985 nm	34-44 %	10 nm NCs in 420 nm MSs	80% after 30 min (H_2O)	TPA-excited PL	2024	**This work**

References

1 Q. Han, W. Wu, W. Liu, Q. Yang and Y. Yang, *Opt. Mater.* 2018, **75**, 880–886.

2 J. Li, Q. Jing, S. Xiao, Y. Gao, Y. Wang, W. Zhang, X. W. Sun, K. Wang and T. He, *J. Phys. Chem. Lett.*, 2020, **11**, 4817–4825.

3 A. Pramanik, K. Gates, Y. Gao, S. Begum and P. Chandra Ray, *J. Phys. Chem. C*, 2019, **123**, 5150–5156.

4 Y. Xu, Q. Chen, C. Zhang, R. Wang, H. Wu, X. Zhang, G. Xing, W. W. Yu, X. Wang, Y. Zhang and M. Xiao, *J. Am. Chem. Soc.*, 2016, **138**, 3761–3768.

5 Y. Wang, X. Li, X. Zhao, L. Xiao, H. Zeng and H. Sun, *Nano Lett.*, 2016, **16**, 448–453.

6 W. Chen, S. Bhaumik, S. A. Veldhuis, G. Xing, Q. Xu, M. Grätzel, S. Mhaisalkar, N. Mathews and T. C. Sum, *Nat. Commun.*, 2017, **8**, 1–9.

7 I. D. Skurlov, W. Yin, A. O. Ismagilov, A. N. Tcypkin, H. Hua, H. Wang, X. Zhang, A. P. Litvin and W. Zheng, *Nanomaterials*, 2022, **12**, 1–16.

8 J. Li, Z. Guo, S. Xiao, Y. Tu, T. He and W. Zhang, *Inorg. Chem.*, 2022, **61**, 4735–4742.

9 A. Pramanik, S. Patibandla, Y. Gao, K. Gates and P. C. Ray, *JACS Au*, 2021, **1**, 53–65.

10 M. M. Kim, J. H. Kim, M. M. Kim, C. S. Kim, J. W. Choi, K. Choi, J. H. Lee, J. Park, Y.-C. Kang, S.-H. Jin and M. Song, *J. Ind. Eng. Chem.*, 2020, **88**, 84–89.

11 T. Gu, J. Zhong, M. Ge, R. Shi, L. He and P. Bai, *J. Colloid Interface Sci.*, 2024, **657**, 580–589.

12 J. Park, K. Y. Jang, S. H. Lee, D.-H. Kim, S.-H. Cho and T.-W. Lee, *Chem. Mater.*, 2023, **35**, 6266–6273.

13 X. Feng, X. Zhang, J. Huang, R. Wu, Y. Leng and Z. Chen, *Anal. Chem.*, 2022, **94**, 5946–5952.

14 T. Yang, Y. Zhu, X. Yang and J. Shen, *Adv. Mater. Interfaces*, 2022, **9**, 2200571.

15 M. N. An, S. Park, R. Brescia, M. Lutfullin, L. Sinatra, O. M. Bakr, L. De Trizio and L. Manna, *ACS Energy Lett.*, 2021, **6**, 900–907.

16 X. Li, W. Cai, H. Guan, S. Zhao, S. Cao, C. Chen, M. Liu and Z. Zang, *Chem. Eng. J.*, 2021, **419**, 129551.

17 J. An, M. Chen, G. Liu, Y. Hu, R. Chen, Y. Lyu, S. Sharma and Y. Liu, *Anal. Bioanal. Chem.*, 2021, **413**, 1739–1747.

18 Q. Zhang, B. Wang, W. Zheng, L. Kong, Q. Wan, C. Zhang, Z. Li, X. Cao, M. Liu and L. Li, *Nat. Commun.*, 2020, **11**, 31.

19 P. Chen, Y. Liu, Z. Zhang, Y. Sun, J. Hou, G. Zhao, J. Zou, Y. Fang, J. Xu and N. Dai, *Nanoscale*, 2019, **11**, 16499–16507.

20 S. Li, D. Lei, W. Ren, X. Guo, S. Wu, Y. Zhu, A. L. Rogach, M. Chhowalla and A. K. Y. Jen, *Nat. Commun.*, 2020, **11**, 1–8.

21 N. Ding, D. Zhou, X. Sun, W. Xu, H. Xu, G. Pan, D. Li, S. Zhang, B. Dong and H. Song, *Nanotechnology*, 2018, **29**, 345703.

22 D. N. Dirin, L. Protesescu, D. Trummer, I. V. Kochetygov, S. Yakunin, F. Krumeich, N.

P. Stadie and M. V. Kovalenko, *Nano Lett.*, 2016, **16**, 5866–5874.

23 H. Wang, S. Lin, A. Tang, B. P. Singh, H. Tong, C. Chen, Y. Lee, T. Tsai and R. Liu, *Angew. Chemie Int. Ed.*, 2016, **55**, 7924–7929.

24 W.-L. Huang, W.-H. Liao and S.-Y. Chu, *ACS Appl. Mater. Interfaces*, 2023, **15**, 41151–41161.

25 Z. Pan, X. Zhu, T. Xu, Q. Xie, H. Chen, F. Xu, H. Lin, J. Wang and Y. Liu, *Appl. Sci.*, 2023, **13**, 7529.

26 Z. Zheng, L. Liu, F. Yi and J. Zhao, *J. Lumin.*, 2019, **216**, 116722.

27 W.-L. Huang and S.-Y. Chu, *Ceram. Int.*, 2023, **49**, 15802–15810.

28 V. Malgras, S. Tominaka, J. W. Ryan, J. Henzie, T. Takei, K. Ohara and Y. Yamauchi, *J. Am. Chem. Soc.*, 2016, **138**, 13874–13881.

29 L.-C. Chen, L.-W. Chao, C.-Y. Xu, C.-H. Hsu, Y.-T. Lee, Z.-M. Xu, C.-C. Lin and Z.-L. Tseng, *Biosensors*, 2021, **11**, 440.